Integrative Biology

TECHNICAL INNOVATION

View Article Online
View Journal | View Issue

Cite this: *Integr. Biol.*, 2014, 6, 470

Plasma membrane recovery kinetics of a microfluidic intracellular delivery platform†

Armon Sharei,‡ Roberta Poceviciute,‡ Emily L. Jackson, Nahyun Cho, Shirley Mao, George C. Hartoularos, Derek Y. Jang, Siddharth Jhunjhunwala, Alexandra Eyerman, Taylor Schoettle, Robert Langer* and Klavs F. Jensen*

Received 16th October 2013,
Accepted 25th January 2014

DOI: 10.1039/c3ib40215k

www.rsc.org/ibiology

Intracellular delivery of materials is a challenge in research and therapeutic applications. Physical methods of plasma membrane disruption have recently emerged as an approach to facilitate the delivery of a variety of macromolecules to a range of cell types. We use the microfluidic CellSqueeze delivery platform to examine the kinetics of plasma membrane recovery after disruption and its dependence on the calcium content of the surrounding buffer (recovery time ~5 min without calcium *vs.* ~30 s with calcium). Moreover, we illustrate that manipulation of the membrane repair kinetics can yield up to 5× improvement in delivery efficiency without significantly impacting cell viability. Membrane repair characteristics initially observed in HeLa cells are shown to translate to primary naïve murine T cells. Subsequent manipulation of membrane repair kinetics also enables the delivery of larger materials, such as antibodies, to these difficult to manipulate cells. This work provides insight into the membrane repair process in response to mechanical delivery and could potentially enable the development of improved delivery methods.

Insight, innovation, integration

Physical approaches to intracellular delivery could potentially overcome many of the challenges associated with vector-based and chemical delivery methods. However, the mechanism of plasma membrane disruption and recovery in physical methods is poorly understood. We describe a new generation of intracellular delivery devices that are used to characterize the process of membrane disruption/repair. Calcium is identified as an important factor that mediates membrane repair thus providing insight into parameters that may govern the performance of other physical approaches, such as ultrasound, electroporation, fluid shear, and nanowire-based methods. This work could potentially enable the design of more effective delivery systems and thus help overcome some of the challenges of intracellular delivery in both research and clinical applications.

Introduction

Intracellular delivery of macromolecules is a challenge in research and clinical applications. Various methods have been developed to address this issue however each approach has particular advantages and disadvantages. Nanoparticle[1,2] and liposome[3] based approaches, for example, have demonstrated some efficacy in delivering materials to established cell lines, but they often struggle to translate to primary cells, especially stem cells[4] and immune cells,[5] and can suffer from off-target effects. Moreover, the techniques often rely on inefficient endosome escape mechanisms that can lose ~70% of the delivered material.[6,7] Viral vectors can be effective for some gene delivery applications; however, they tend to be limited to nucleic acid delivery and raise safety concerns in clinical applications.[8,9] Alternatively, cell penetrating peptides can be effective for some protein delivery applications although they also suffer from the same endosome escape problems as nanoparticle-based approaches.[10,11]

Physical approaches to delivery are potentially more robust and could overcome some of the challenges associated with vector-based and chemical methods.[12] Electroporation,[13,14] for example, has demonstrated efficacy in previously challenging primary cells. Sonoporation has also begun to show promise in some applications.[15] Because these methods are based on physical disruption of the plasma membrane, they provide direct access to the cell cytoplasm. In contrast, the aforementioned chemical and vector-based techniques typically rely on

Department of Chemical Engineering, Massachusetts Institute of Technology, 77 Massachusetts Ave., Cambridge, MA 02139, USA. E-mail: rlanger@mit.edu, kfjensen@mit.edu

† Electronic supplementary information (ESI) available. See DOI: 10.1039/c3ib40215k

‡ These authors contributed equally to this work.

less efficient endosome escape mechanisms that hinder their ability to translate to different materials and cell types.

The recently described CellSqueeze microfluidic platform has emerged as a robust physical approach to intracellular delivery.[16–19] Mechanically inducing disruption of the plasma membrane enables passive diffusion of the target material into the cell cytoplasm. This approach obviates the need for exogenous materials or fields to facilitate delivery and has demonstrated its efficacy in cell reprogramming (10–100× improved efficiency)[19] and single-molecule imaging applications.[20] However, the mechanism of membrane disruption and repair is poorly understood.

In this work, we develop improved versions of the platform and studied membrane repair in response to cell squeezing. Specifically, we conduct experiments to elucidate the potential dependence of the repair process on calcium. Other membrane repair studies have indicated that calcium signaling is an important component in repairing large membrane disruptions, while it does not necessarily participate in the closure of smaller pores (<0.2 μm).[21,22] Thus, analysis of the calcium dependence of the repair process would potentially support the membrane disruption/repair delivery hypothesis (*versus* endocytosis for example), provide some insight into the size range of the disruptions, and help guide the development of more effective delivery methods.

Experimental

Cell culture

HeLa cells were cultured in Dulbecco's Modified Eagle Medium (DMEM) (Invitrogen, USA) supplemented with 10% fetal bovine serum (Invitrogen, USA) and 1% penicillin/streptomycin (Sigma, USA). One day before delivery, 3×10^6 cells were seeded into a 750 cm^2 tissue culture flask. Before the experiment, cells were detached from the tissue culture flask: old medium was removed; the cells were washed with 5 mL of PBS (Invitrogen, USA), incubated with 5 mL of 0.5% trypsin/EDTA (Invitrogen, USA) at 37 °C for 10 min, and neutralized with 10 mL of fresh medium. The resulting cell suspension was split equally into as many tubes as there were experimental conditions. The tubes were spun at 800*g* for 5 min, the supernatant was discarded, and the cell pellet was resuspended in a buffer of interest to yield a final cell concentration of 3×10^6 cells per mL.

Delivery procedure

Delivery experiments were conducted as described previously.[23] Briefly, the suspension of cells and delivery material was passed through the device at the desired pressure. Treated cells (60–80 μL per sample) were collected in a 96-well plate and allowed to recover for >5 min at room temperature. Fresh cell culture medium was then added to cells prior to further processing or overnight culture. The microfluidic devices used in these experiments were obtained from SQZ Biotechnologies, USA.

Device comparison

Cell suspensions were prepared in PBS with the following material concentrations: 0.1 mg mL^{-1} 3 kDa cascade blue dextran, 0.1 mg mL^{-1} 70 kDa fluorescein labeled dextran, and 0.05 mg mL^{-1} APC labeled IgG1 isotype control antibody. The cells were passed through the device at three different pressures (30, 50, and 70 psi) using four different device types (10-7, 10-6, 50-6, 10-6×5). Treated cells were incubated for ~5 min post-delivery to ensure appropriate membrane recovery. FACS analysis was performed the same day. Three controls were used: untreated cells not exposed to the dye solution, untreated cells exposed to the dye solution, and cells treated at 30 psi without exposure to the dye solution.

Buffer comparison

Cell suspensions were prepared in three buffers: PBS, DMEM, and a third buffer (1.8 mM $CaCl_2$ in PBS, 1.8 mM EDTA in PBS, 2.7 mM NaCl in PBS, or medium). Delivery materials were added at the concentrations indicated previously. The cells were passed through the device at four different pressures (30, 50, 70, and 100 psi). FACS analysis was performed the next day. Two controls were used: untreated cells not exposed to the dye solution and untreated cells exposed to the dye solution.

Calcium dosage

Cell suspensions were prepared in four buffers: PBS, 1.8 mM $CaCl_2$ in PBS, 0.9 mM $CaCl_2$ in PBS, and 0.18 mM $CaCl_2$ in PBS. Delivery materials were added at the concentrations indicated previously. The cells were passed through the device at four different pressures (30, 50, 70, and 100 psi). FACS analysis was performed the next day. Two controls were used: untreated cells not exposed to the dye solution and untreated cells exposed to the dye solution.

Membrane recovery kinetics

The cell suspension was prepared in a single buffer (PBS, DMEM, or 1.8 mM $CaCl_2$ in PBS) in the absence of any delivery material. For a zero time point, the delivery material was added to yield the final dye concentration and immediately treated by the device at 70 psi. For subsequent time points, the cell suspension alone was passed through the device at 70 psi, and the dye solution was added at set time points (15 s, 30 s, 45 s, 1 min, 1.5 min, 2 min, 3 min, 5 min, and 10 min) to yield the same final dye concentrations indicated previously. Treated cells were incubated with the dyes for >5 min post-exposure. In experiments with HeLa cells, FACS analysis was performed the next day, whereas in experiments with naïve murine T cells FACS analysis was performed the same day (due to the challenge of culturing primary naïve T cells). Three controls were used: untreated cells not exposed to the dye solution, untreated cells exposed to the dye solution, and cells treated at 70 psi not exposed to the dye solution.

FACS sample preparation and analysis

Samples were prepared in a 96-well v-bottom plate and washed with 150 μL of PBS per well. The cells were suspended in FACS

buffer (3% FBS, 1% pluronics, 1% PI in DPBS, 100 μL per well) prior to analysis.

Samples were processed on a FACS Canto or LSR Fortessa analyzer (Becton-Dickinson, USA). Results were analyzed using FACS Diva (Becton-Dickinson, USA) and FlowJo software (Treestar, USA).

T cell isolation

Spleens were harvested from male C57BL6 mice (Jackson Labs, USA) at 6–12 weeks of age. Spleens were mechanically disrupted by grinding using a pair of serrated tweezers to yield a cell suspension of splenocytes. The suspension was passed through a 40 μm filter to eliminate any aggregates, and red blood cell lysis was performed according to instructions (Cat no. 00-4333-57, eBioscience, USA). After lysis, cells were concentrated to 2×10^8 cells per mL. T cells were isolated using the EasySep T cell isolation kit with the manufacturer's protocol (Cat no. 19851, StemCell Technologies, USA). The separation process is a negative selection, thus the isolated T cells did not have any magnetic particles bound to them. Purified T cells were then suspended in the desired buffer for device treatment.

Results and discussion

Performance characterization

As described previously, the CellSqueeze platform relies on rapid mechanical deformation of a cell as it passes through a microfluidic constriction to induce membrane disruption.[19] Although current manifestations of the system require each cell to be treated individually by the constriction, parallelization of the approach has enabled us to operate the system with high throughputs (50 000–500 000 cells per second). This parallelization strategy can lead to heterogeneity in treatment across channels as the fluid flow profile through different channels could be affected by their relative positions. As the cell speed has been shown to be an important parameter in determining the delivery efficiency and cell viability,[19] differences in cell speed across channels can potentially lead to significant heterogeneity in the treated cell population. To address this concern, we developed a new generation of devices designed to increase throughput and treatment homogeneity. The device design, described in Fig. 1a and b, divides the cell flow in two stages and is symmetrical. Compared to the previously described system, these devices have higher throughput (~6× at a given operating pressure), can accommodate cell flow in either direction, and provide more homogenous treatment (Fig. S1 and Table S1, ESI†). The measured cell recovery rates for these device designs were over 90% (Fig. S2, ESI†).

Having reduced process variability due to differential flow speeds, we conducted characterization studies of the new designs using HeLa cells as a model. In these studies, we designed devices with different constriction lengths, widths and number of constrictions in series. The design nomenclature is defined as (constriction length) − (constriction width) × (number of constrictions in series). Fluorescently labeled dextran polymers and isotype control antibodies were used to assess the delivery efficiency for different sized target molecules (Fig. 2). For a given constriction width, increasing channel length or number of constrictions in series increases the delivery efficiency and reduces the cell viability. Increasing operating pressure (or cell speed) also increased the delivery efficiency across designs (Fig. S3 and S4, ESI†). The 10-6×5 design appears to be harsher than the 50-6 design (*i.e.* providing higher delivery and lower viability), suggesting that placing multiple 10 μm length constrictions in series is more effective for membrane disruption than generating a single constriction of equivalent total length. In comparison to the previously reported design scheme,[19] the devices described herein also exhibited a more uniform distribution of delivery material (Fig. 2), suggesting that heterogeneity amongst the treated population may have been partially mitigated by this approach.

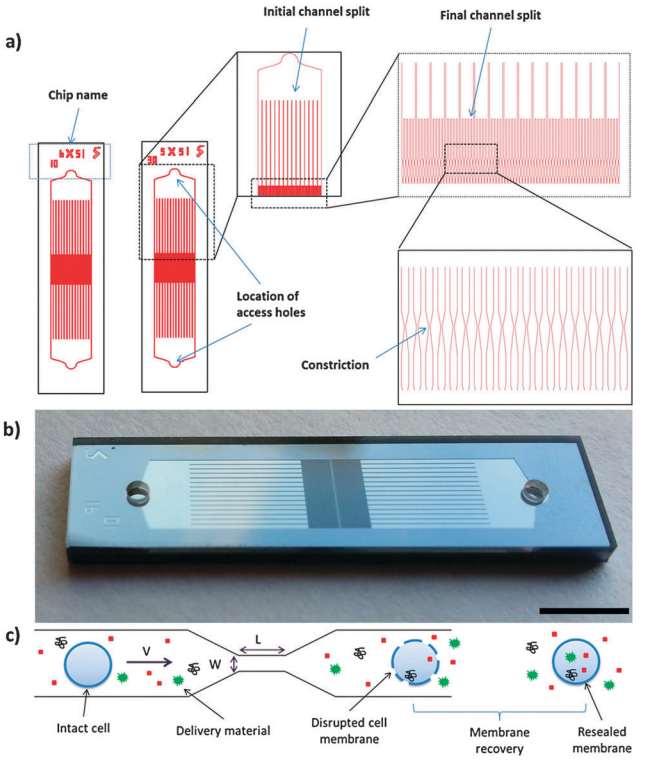

Fig. 1 Overview of device design and investigated parameters. (a) A schematic of the device design and the relative positioning of individual channels. Each device is symmetrical and consists of two access holes on each side for cells to enter and exit the device. The flow is first split into 15 separate channels and subsequently further subdivided into 5 channels, each containing a constriction. The width of the channel prior to the constriction point is 30 μm. (b) Image of a device implemented in glass and silicon. Scale bar is 2 mm. (c) An illustration of the delivery process. The membrane of the target cell is disrupted after treatment by the constriction and the material in the surrounding buffer can diffuse into the cell for the duration of the membrane recovery phase.

Calcium dependent delivery

To better understand the process of membrane recovery post-treatment, we designed experiments to characterize recovery kinetics and its dependence on buffer composition, specifically

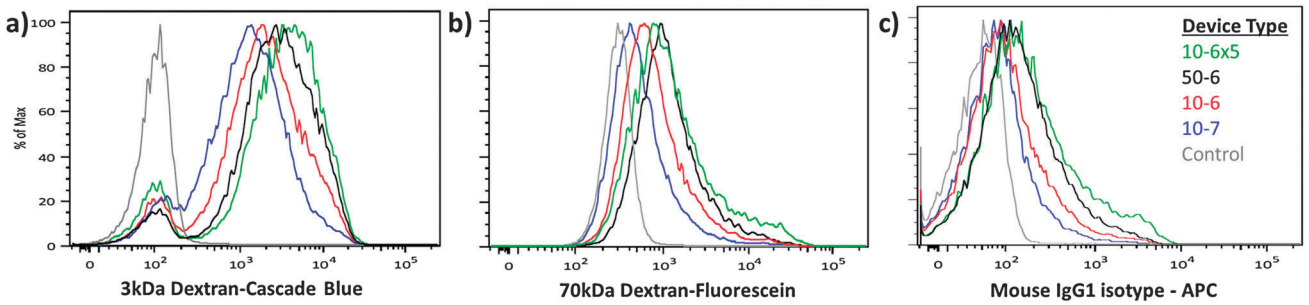

Fig. 2 Delivery performance across device designs. HeLa cells were treated by 4 different device designs to deliver: (a) cascade blue conjugated 3 kDa dextran, (b) fluorescein conjugated 70 kDa dextran, and (c) an APC conjugated IgG1 isotype control antibody. The three materials were delivered simultaneously and the results were measured by flow cytometry. 10-6×5 devices demonstrated the highest delivery efficiency, while 10-7 devices demonstrated the lowest efficiency of the designs tested. Control samples were incubated with the delivery mixture for the duration of the experiment to account for autofluorescence, endocytosis and surface binding of the target materials. The displayed data are obtained from a representative case of our triplicate data set (Fig. S3 and S4, ESI†).

calcium content. Previous studies have reported that the closure of physically generated membrane disruptions could be governed by thermodynamic rearrangement of the cell membrane or by calcium mediated signaling to active membrane recovery processes.[21] These studies also indicate that holes greater than ~200 nm in size are primarily addressed through active recovery mechanisms while those below that range are primarily addressed through thermodynamic rearrangement. We conducted experiments in buffers with and without calcium to gauge the dependence of delivery on the presence of the ion.

The results in Fig. 3 demonstrate that cells treated by a 50-6 device in PBS receive more dextran than those treated in PBS with 1.8 mM calcium (physiological calcium concentration is 1–2 mM[24,25]). A similar difference is observed when comparing full culture media and DMEM to PBS, indicating that their calcium content is likely the major determinant of the observed delivery behaviour (Fig. S5, ESI†). Further studies indicated that the aforementioned calcium response is dose dependent (Fig. 3c) and cannot be recreated by the addition of an alternative cation, such as sodium (Fig. S7, ESI†). These results are consistent with previous reports of calcium mediated membrane repair.[21,26]

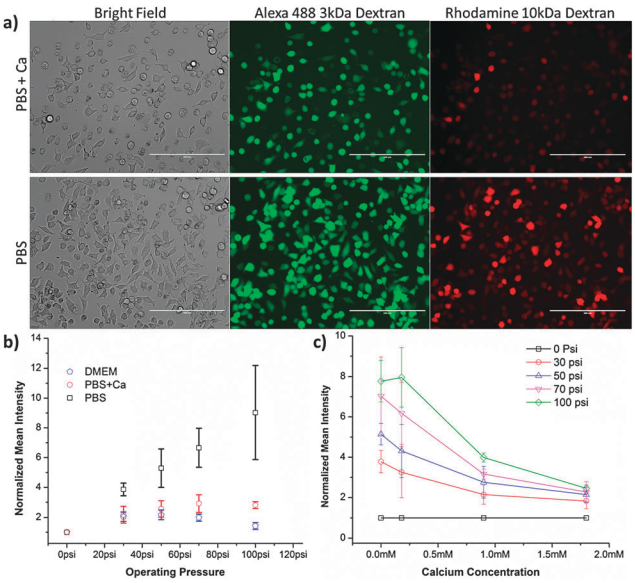

Fig. 3 Delivery by cell squeezing is calcium dependent. (a) Representative images from cells treated by a 50-6 device. Images were obtained on the day of treatment. Intracellular delivery of 3 kDa Alexa Fluor 488 conjugated dextran and 10 kDa tetramethyl rhodamine conjugated dextran was measured by fluorescence microscopy. The PBS + Ca buffer consisted of PBS supplemented with 1.8 mM of calcium. Scale bars are 200 μm. (b) Normalized delivery intensity of HeLa cells treated in different buffers. Experiments were conducted in PBS, PBS + Ca, and Dulbecco's modified eagle medium (DMEM). Corresponding viability data are presented in Fig. S6 (ESI†). (c) Normalized delivery intensity of HeLa cells treated in PBS containing different concentrations of calcium. The experiments were conducted across different operating pressures to confirm that the results were consistent across conditions. The mean intensity of cascade blue conjugated 3 kDa dextran was measured by flow cytometry and normalized against the control to account for background effects (*e.g.* endocytosis and surface binding). Error bars represent 2 standard deviations among triplicates.

Membrane recovery kinetics

To confirm that the observed calcium effects are correlated to membrane repair behaviour we examined the rate of repair in response to membrane disruption in different buffers. The CellSqueeze platform was suitable for these studies as the treatment duration for a given sample is 0.5–10 s, thereby allowing for follow-up soon after membrane disruption. In these experiments, cells were initially treated by the device in the absence of dextran and subsequently exposed to dextran at defined time points. The intensity of dextran fluorescence in cells at a given time point should correlate to the extent of membrane disruption that persisted since the initial treatment. These data demonstrate that cells treated in the presence of calcium appear to seal their membranes within 15–30 s, whereas those treated in PBS alone are not fully closed even 3 min after treatment (Fig. 4a and b). This delay in membrane repair could account for the difference in delivery efficiency described earlier (Fig. 3) and was observed in both the 10-6 and 50-6 designs (Fig. 4c).

These data suggest that membrane recovery post-treatment is an active, calcium-mediated, process. Indeed, further studies with

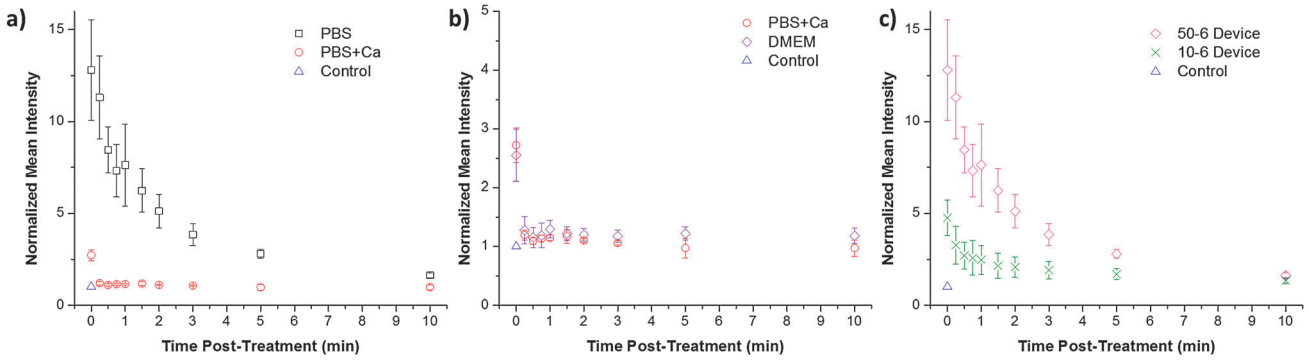

Fig. 4 Pore closure kinetics are calcium dependent. (a) Normalized intensity of HeLa cells treated in the absence of dyes and subsequently exposed to cascade blue conjugated 3 kDa dextran at the specified time points. PBS, PBS supplemented with 1.8 mM of calcium, and (b) DMEM were used as buffers during these experiments. (c) Treatment of HeLa cells by a 50-6 and a 10-6 device is also compared in a PBS buffer. The mean intensity of cascade blue conjugated 3 kDa dextran was measured by flow cytometry and normalized against the control to account for background effects (*e.g.* endocytosis and surface binding). Error bars represent 2 standard deviations among triplicates. Corresponding viability data are presented in Fig. S8 (ESI†).

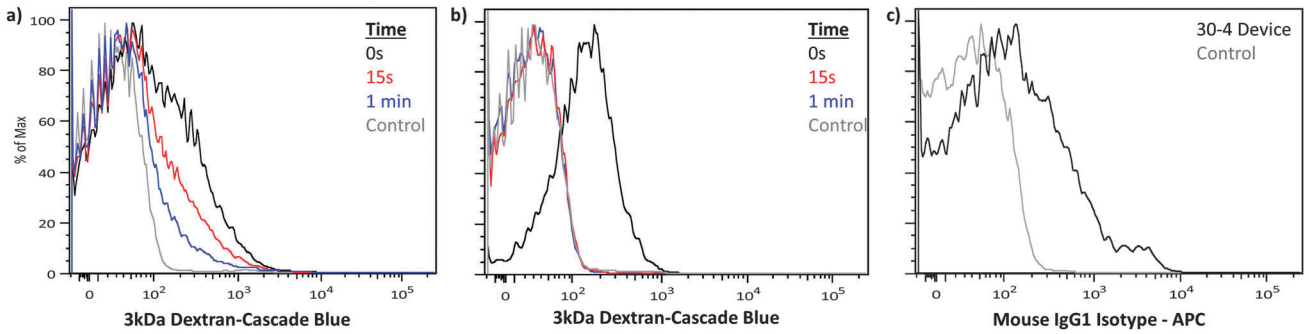

Fig. 5 Translation to primary naïve murine T cells. Naïve murine T cells were treated by a 30-4 device in the absence of dyes and subsequently exposed to cascade blue conjugated 3 kDa dextran at the specified times. (a) PBS and (b) PBS supplemented with 1.8 mM of calcium were used as delivery buffers to compare membrane recovery kinetics. (c) Delivery of APC conjugated IgG1 isotype control antibodies to naïve murine T cells by a 30-4 device run on ice. Control samples were incubated with the delivery mixture for the duration of the experiment to account for autofluorescence, endocytosis and surface binding of the target materials. The displayed data were obtained from a representative case of our triplicate data set by flow cytometry (Fig. S10, ESI†).

cells treated at refrigerated temperatures (*i.e.* on ice) indicated that membrane repair may be retarded relative to treatment under ambient conditions (Fig. S9, ESI†). Although changes in temperature can influence many cell properties, low temperatures do reduce cell activity[27] and thus these results would be consistent with the active membrane recovery hypothesis.

To examine the applicability of these findings to primary cells, we conducted experiments in naïve T cells derived from the lymph nodes and spleen of C57BL6 mice. These experiments demonstrate that a similar calcium (Fig. 5a and b, Fig. S10, ESI†) and temperature dependence (Fig. S11, ESI†) is observed in primary naïve T cells. This insight into membrane recovery enabled us to develop protocols that facilitate the delivery of antibodies to primary naïve T cells with up to 54% efficiency, while maintaining 56% viability (Fig. 5c and Fig. S12, ESI†).

Conclusions

In this work, we describe a new generation of intracellular delivery devices that provide higher throughput (~6×) and more uniform treatment (Fig. 1, Fig. S1 and Table S1, ESI†). These devices are used to characterize the process of membrane disruption/repair and its dependence on constriction geometry, flow rate, and buffer composition. Calcium is identified as an important parameter that mediates membrane repair thus indicating that the disruptions generated by this technique are potentially over 200 nm in size[21] (Fig. 3). Characterization of the kinetics of delivery and membrane repair is of value to the field as it provides insight into parameters that may govern the performance of other physical approaches to intracellular delivery, such as ultrasound,[15] fluid shear,[28] and nanowire-based[29] methods. Indeed these data indicate that the calcium composition of the buffer (Fig. 3), temperature (Fig. S9 and S11, ESI†), and incubation time post-treatment (Fig. 4) are important determinants of treatment efficacy.

The gained insight into membrane repair kinetics enabled us to evolve our technique to potentially address the challenge of protein delivery to T cells (Fig. 5). Moreover, the consistency of the observed phenomena across HeLa cells and naïve T cells, coupled with the reported ubiquity of the calcium-mediated membrane repair mechanism,[21,22] would suggest that the aforementioned parameters are potentially relevant to a broad range of cell types.

Our work highlights the importance of membrane recovery and how careful manipulation of delivery conditions can improve performance without sacrificing cell viability. The described experiments also underscore the potential utility of this approach in studying membrane repair kinetics and its associated pathways, such as vesicular exocytosis,[30] to better understand repair mechanisms in healthy and diseased cells. Future work with this platform could help elucidate the potential role of other ions and proteins, such as magnesium and calmodulin,[31] through siRNA gene knockdown, antibody-based pathway inhibition, and buffer composition studies. A deeper understanding of the membrane repair process could potentially enable the design of more effective delivery methods and thus help overcome some of the challenges of intracellular delivery in both research and clinical applications.

Conflict of interest

A.S., R.L., and K.F.J. have a financial interest in SQZ Biotechnologies.

Acknowledgements

This work was supported by National Institutes of Health Grants RC1 EB011187-02 and R01GM101420-01A1, the Kathy and Curt Marble Cancer Research Fund and partially by the National Cancer Institute Cancer Center Support (Core) Grants P30-CA14051 and MPP-09Call-Langer-60.

Notes and references

1 I. I. Slowing, B. G. Trewyn and V. S. Y. Lin, *J. Am. Chem. Soc.*, 2007, **129**, 8845–8849.
2 D. W. Pack, A. S. Hoffman, S. Pun and P. S. Stayton, *Nat. Rev. Drug Discovery*, 2005, **4**, 581–593.
3 Z. Joseph, *Adv. Drug Delivery Rev.*, 1997, **27**, 17–28.
4 J. Zoldan, A. K. R. Lytton-Jean, E. D. Karagiannis, K. Deiorio-Haggar, L. M. Bellan, R. Langer and D. G. Anderson, *Biomaterials*, 2011, **32**, 7793–7800.
5 V. F. I. Van Tendeloo, P. Ponsaerts, F. Lardon, G. Nijs, M. Lenjou, C. Van Broeckhoven, D. R. Van Bockstaele and Z. N. Berneman, *Blood*, 2001, **98**, 49–56.
6 A. K. Varkouhi, M. Scholte, G. Storm and H. J. Haisma, *J. Controlled Release*, 2011, **151**, 220–228.
7 G. Sahay, W. Querbes, C. Alabi, A. Eltoukhy, S. Sarkar, C. Zurenko, E. Karagiannis, K. Love, D. Chen and R. Zoncu, *Nat. Biotechnol.*, 2013, **31**, 653–658.
8 R. Waehler, S. J. Russell and D. T. Curiel, *Nat. Rev. Genet.*, 2007, **8**, 573–587.
9 Y.-C. Hu, *Curr. Gene Ther.*, 2008, **8**, 54–65.
10 B. Gupta, T. S. Levchenko and V. P. Torchilin, *Adv. Drug Delivery Rev.*, 2005, **57**, 637–651.
11 T. Endoh and T. Ohtsuki, *Adv. Drug Delivery Rev.*, 2009, **61**, 704–709.
12 S. Brunner, E. Fürtbauer, T. Sauer, M. Kursa and E. Wagner, *Mol. Ther.*, 2002, **5**, 80–86.
13 S. Li, *Curr. Gene Ther.*, 2004, **4**, 309–316.
14 M. Fox, D. Esveld, A. Valero, R. Luttge, H. Mastwijk, P. Bartels, A. van den Berg and R. Boom, *Anal. Bioanal. Chem.*, 2006, **385**, 474–485.
15 D. L. Miller, S. V. Pislaru and J. F. Greenleaf, *Somatic Cell Mol. Genet.*, 2002, **27**, 115–134.
16 T. Nawy, *Nat. Methods*, 2013, **10**, 198.
17 , *Nature*, 2013, **493**, 581.
18 P. Pamies, *Nat. Mater.*, 2013, **12**, 178.
19 A. Sharei, J. Zoldan, A. Adamo, W. Y. Sim, N. Cho, E. Jackson, S. Mao, S. Schneider, M. J. Han, A. Lytton-Jean, P. A. Basto, S. Jhunjhunwala, J. Lee, D. A. Heller, J. W. Kang, G. C. Hartoularos, K. S. Kim, D. G. Anderson, R. Langer and K. F. Jensen, *Proc. Natl. Acad. Sci. U. S. A.*, 2013, **110**, 2082–2087.
20 J. Lee, A. Sharei, W. Y. Sim, A. Adamo, R. Langer, K. F. Jensen and M. G. Bawendi, *Nano Lett.*, 2012, **12**, 6322–6327.
21 P. L. McNeil and R. A. Steinhardt, *Annu. Rev. Cell Dev. Biol.*, 2003, **19**, 697–731.
22 P. L. McNeil and T. Kirchhausen, *Nat. Rev. Mol. Cell Biol.*, 2005, **6**, 499–505.
23 A. Sharei, N. Cho, S. Mao, E. Jackson, R. Poceviciute, A. Adamo, J. Zoldan, R. Langer and K. F. Jensen, *J. Visualized Exp.*, 2013, **81**, e50980, DOI: 10.3791/50980.
24 L. Larsson and S. Ohman, *Clin. Chem.*, 1978, **24**, 1962–1965.
25 M. M. Dvorak, A. Siddiqua, D. T. Ward, D. H. Carter, S. L. Dallas, E. F. Nemeth and D. Riccardi, *Proc. Natl. Acad. Sci. U. S. A.*, 2004, **101**, 5140–5145.
26 A. Reddy, E. V. Caler and N. W. Andrews, *Cell*, 2001, **106**, 157–169.
27 I. H. Pastan and M. C. Willingham, *Annu. Rev. Physiol.*, 1981, **43**, 239–250.
28 D. M. Hallow, R. A. Seeger, P. P. Kamaev, G. R. Prado, M. C. LaPlaca and M. R. Prausnitz, *Biotechnol. Bioeng.*, 2008, **99**, 846–854.
29 A. K. Shalek, J. T. Robinson, E. S. Karp, J. S. Lee, D.-R. Ahn, M.-H. Yoon, A. Sutton, M. Jorgolli, R. S. Gertner and T. S. Gujral, *Proc. Natl. Acad. Sci. U. S. A.*, 2010, **107**, 1870–1875.
30 R. A. Steinhardt, G. Bi and J. M. Alderton, *Science*, 1994, **263**, 390–393.
31 J. V. Gerasimenko, O. V. Gerasimenko and O. H. Petersen, *Curr. Biol.*, 2001, **11**, R971–R974.